A Virtual Environment and Model of the Eye for Surgical Simulation

Mark A. Sagar[1], David Bullivant[2], Gordon D. Mallinson[1], Peter J. Hunter[2]
The University of Auckland, New Zealand
Ian W. Hunter[3]
McGill University, Canada

ABSTRACT

An anatomically detailed 3-D computer graphic model of the eye and surrounding face within a virtual environment has been implemented for use in a surgical simulator. The simulator forms part of a teleoperated micro-surgical robotic system being developed for eye surgery. The model has been designed to both visually and mechanically simulate features of the human eye by coupling computer graphic realism with finite element analysis.

The paper gives an overview of the system with emphasis on the graphical modelling techniques and a computationally efficient framework for representing anatomical details of the eye and for finite element analysis of the mechanical properties. Examples of realistic images coupled to a large deformation finite element model of the cornea are presented. These images can be rendered sufficiently fast for the virtual reality application.

CR Descriptors: I.3.7 [**Computer Graphics**]: Three-Dimensional Graphics and Realism --- *Virtual Reality;* I.6.3 [**Simulation and Modelling**]: Applications.

1. INTRODUCTION

We are developing a teleoperated micro-surgical robot for eye surgery. In order to provide simulation for training and to assist during surgery a virtual environment has been implemented as part of the system. During a simulation, the surgeon operates the robot in exactly the same way as it would be used when performing actual surgery.

[1] Department of Mechanical Engineering,
[2] Department of Engineering Science, The University of Auckland, Private Bag 92019, Auckland, New Zealand.
[3] Biorobotics Laboratory, Department of Biomedical Engineering, McGill University, Montreal, Canada.
Emails: ma.sagar@auckland.ac.nz, d.bullivant@auckand.ac.nz, g.mallinson@auckland.ac.nz, p.hunter@auckland.ac.nz, ian@biorobotics.mcgill.ca

This paper describes our efforts to create anatomical realism in a virtual environment for eye surgery involving visual and mechanical simulation. It provides a framework for the coupling of computer graphics for visual realism with finite element analysis and input from physical instruments.

The creation of a surgical virtual environment to both aid surgeons during operations and provide simulations for training opens up many exciting possibilities. The surgical procedure will be able to be viewed and visualized in new ways providing a new level of surgical experience. During surgery, the predicted mechanical and optical consequences of a particular incision and the optimization of tasks based on underlying mathematical models of tissue can be presented to the surgeon graphically. Operations can be recorded and analysed, and sent to colleagues in electronic form. Before or after surgery the environment can be used as a training simulator.

The use of interactive 3-D graphic modelling for surgical simulation has been gaining popularity. Examples include an endoscopic simulator containing a simplified representation of the colon [1], a system for simulation of tendon transfer operations with simplified geometry [3] and graphic models for simulations generated from CT and MRI scans [4]. Work is also being done on simulating certain laparoscopic surgical procedures in real time [14].

Only a few papers have been published on the realistic display of finite element based biomechanical simulations. Examples are a plastic surgery planning system in which a 3-D surface scan of a patient's face is meshed with finite elements and the displacements resulting from incisions deform the surface scan to show the predicted effects [12] and a simulation of skeletal muscles to provide images for computer animation [2]. In neither case was the time taken to generate each image an issue.

Eye structures such as the sclera and cornea have previously been modelled using analytical techniques [6] or finite element numerical analysis [10,13] but these have used linear elastic deformation theory. Since the cornea is anisotropic and nonlinearly elastic and undergoes large deformations, we have used large deformation elasticity theory with orthotopic and nonlinear material properties in the finite element model.

For the simulation to be most convincing, the surgeon should ideally perform the operation in exactly the same manner and use the same tools as in the actual operation. The display of the subject must look as realistic as possible and the user should be able to manipulate and have a 3-D spatial understanding of the environment. To simulate eye surgery realistically requires the

construction of an accurate model of the eye with biomechanically based features. Visually, more realism normally implies more complexity and hence more computer time to generate the image. The graphic modelling challenge is to find fast, simple methods to give the illusion of complexity - which must continue under close scrutiny. Using the finite element approach, the graphic modelling must be coupled with analysis for the key anatomical features being operated on.

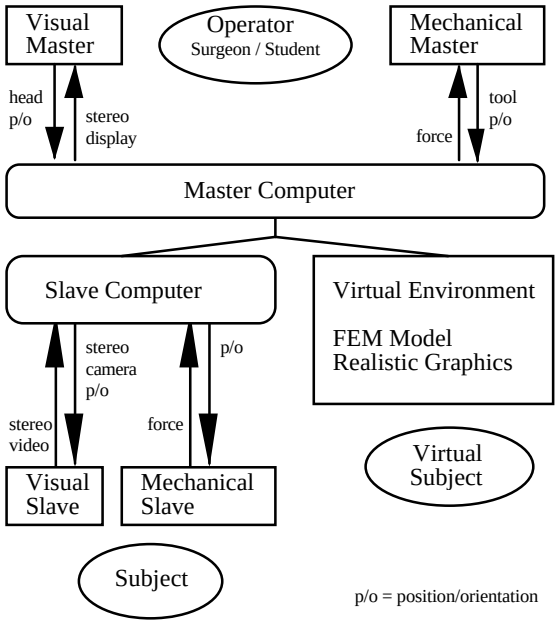

Figure 1: Block diagram of the micro-surgical robotic system.

2. OVERVIEW OF THE MICRO-SURGICAL ROBOTIC SYSTEM

Micro-surgery is currently performed by skilled surgeons often using hand crafted tools, where surgical intervention is limited by the dexterity of the surgeon and the available workspace. In the teleoperated micro-surgical robotic system currently being developed, a micro-surgical robot (MSR-1) will perform delicate eye operations under the guidance of a surgeon [8].

The micro-surgical system (see Figure 1) is composed of mechanical and visual master and slave subsystems. The surgeon grasps a handle (such as a micro-scalpel handle) which forms part of the micro-surgical mechanical master. Movements of this handle are monitored by six position transducers and fed to the master computer, where tremor is filtered prior to transmission to the slave computer which reproduces the same movement but scaled down by up to 100 times. The slave micro-surgical robot can hold a variety of micro-tools (diamond knives, probes etc). Forces measured by six transducers in the slave micro-surgical robot are scaled up and reflected back to the six actuators in the mechanical master which then exerts corresponding forces on the handle giving force feedback. The six-axis position/orientation of the surgeon's head (helmet) is used to control the slave stereo camera head. Stereo images from the slave cameras are transmitted back to the surgeon and displayed on either a head mounted display (HMD) or on a large high resolution video rear projection screen.

The modular nature of the Master-Slave arrangement allows the images and forces fed back to the master from the slave to be replaced (or aided) by visual and mechanical computer simulations.

The virtual reality system replaces (or combines) the camera image with computer graphics generated from the eye model. Forces felt by the robot are determined using a finite element model of the tissue and are fed back to the operator via the force reflecting master. In this way both visual and mechanical simulation are achieved, with the surgeon using the same physical equipment as in an actual operation. The graphics can be displayed on either a stereo monitor, video projection screen or HMD.

3. GENERAL ANATOMY OF THE EYE

As described in medical texts the eyeball can be considered as being composed of the segments of two slightly deformed spheres of different radii. It consists of three concentric layers which enclose its contents (see Figure 2):

(1) The outermost fibrous layer maintains the shape of the eyeball and is called the sclera save for a transparent section at the front called the cornea which is the major area of refraction for light entering the eye.

(2) The pigmented middle layer is vascular and nutritive in function and comprises the choroid, ciliary body and iris which is visible through the cornea.

(3) The innermost layer is the retina, which consists of nerve elements and is the visually receptive area of the eye.

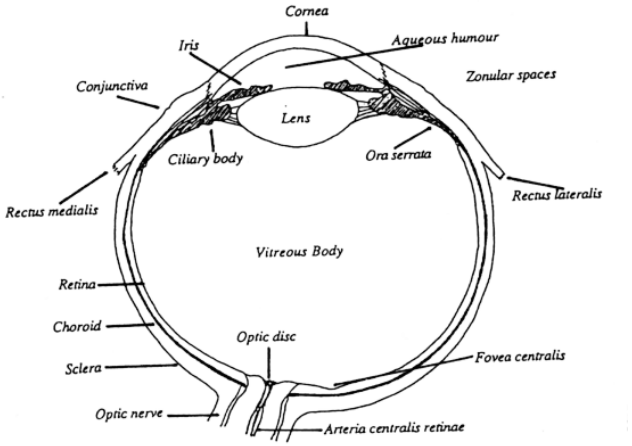

Figure 2: The components of the eye.

4. THE 3-D COMPUTER GRAPHIC EYE MODEL

The eye has previously been modelled for computer graphics applications, mainly as part of facial models for animation sequences. Detail has usually been unnecessary because the face has been viewed from a distance, thus specific features of the eye have been simplified or omitted. The iris has normally been treated as a one or two colour annulus and the eyelids and eyelashes (if any) have been simple curves and surfaces, for example [9]. No reference has been found which models the interior of the eye.

The aim here was to produce a fast accurate 3-D model of the eye which holds its detailed appearance even on close up. We chose 10 Hz to be the minimum acceptable display rate for our initial virtual reality applications.

It was necessary to make the model modular, so that aspects of the model, both graphical and analytical could be refined independently as development proceeded, and to allow aspects of the model to be animated such as making the eyelids blink, the eyeball rotate in its orbit and the pupil constrict or dilate.

Another concern was to give the graphics generated from the model parametric complexity so that the same 'model' could be used for rendering at different speeds. Different levels of detail (LOD) can be individually assigned to components of the model.

The above considerations led to a graphical modelling approach based on 3-D graphics primitives rendered by a workstation's graphics pipeline. Quite realistic images and lighting can be generated without the need for more versatile but more compute intensive rendering options such as ray tracing.

A general view of the current model is shown in Figure 6. The eyeball can be seen together with the arrangement of the surface patches used to represent the skin.

5. GRAPHICAL FEATURES OF THE MODEL

5.1 The sclera and cornea

The cornea is more highly curved than and protrudes from the sclera, which is white and smooth except where the tendons of the ocular muscles are attached. Both are displayed using relatively few polygons which are Gouraud shaded to produce a smoothed effect. For corneal surgery the specific geometry of a particular cornea will be obtained using laser based confocal microscopic imaging systems being developed for use in the micro-surgical robotic system [8].

5.2. The iris

The iris is the gemlike adjustable diaphragm around the pupil which controls the amount of light entering the eye. The colour of the iris ranges from light blue to very dark brown and is due to iridial connective tissue and pigment cells, which are often distributed irregularly producing a flecked appearance. The front surface of the iris can be divided into outer, ciliary, and inner, pupillary zones which often differ in colour and are separated by the collarette, a zigzag line, near which there are many pit like depressions called crypts.

Representing the iris parametrically is difficult due to its complex colours and shapes. The approach adopted was to generate two layers (ciliary and pupillary) of wavy radial fibres with each fibre being a single Gouraud shaded polygon with six or more vertices and colours specified by a colour ramp. The co-radial fibre vertices were given slightly different colours to produce a 3-D curved effect. The ciliary fibres were bounded to the collarette which was generated using a periodic function. The ciliary fibre waviness was increased with Gaussian perturbations near the collarette resulting in the formation of crypts between opposed phases. When the pupil dilates in the model, the ciliary fibres become wavy. The pupillary fibres lie slightly below and have the greatest radial retraction.

An alternative method that we have used to generate the iris has been to apply a texture map (from a close up photograph) to significantly fewer polygons. This speeds up the rendering of the iris on dedicated texture mapping hardware such as Silicon Graphics' Reality Engine. A disadvantage of this approach is that it does not allow the individual components comprising the iris to be manipulated as separate objects. We have chosen a combination of discrete object modelling and texture mapping depending on the level of object manipulation we require and the texture mapping performance of the workstation.

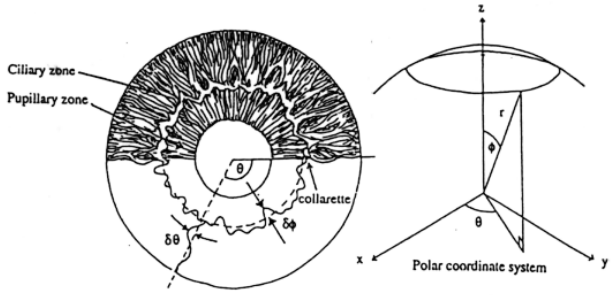

Figure 3: Geometric details of the modelling of the iris.

5.3. The retina and retinal blood vessels

The retina is mainly soft and translucent. Near its centre is an oval yellowish area which has a central depression, the fovea centralis, where visual resolution is the highest. This area contains no retinal blood vessels. About 3 mm nasal to this area is the optic disc where the optic nerve joins the retina. The optic disc is slightly puckered and is pierced by the central retinal blood vessels. Usually pink but much paler than the retina, it may be grey or almost white. The general retinal hue is a bright terracotta red which contrasts sharply with the optic disc.

The central retinal artery divides into two equal branches and again in a few mm, each branch supplying its own 'quadrant' of the retina. The central retinal vein is formed correspondingly. The branching of the artery is usually dichotomous with a 45 to 60 degree angle. Smaller lateral branches may leave at right angles. The vessels are visible as they lie close to the retinal surface.

For retinal surgery, in order to accurately model the retina and retinal blood vessel distribution of a specific patient, it would be necessary to stereoscopically scan the retina obtaining 3-D retinal surface estimation and blood vessel form in a similar manner to [15]. At present we are focusing on corneal surgery and retinal and retinal blood vessel positional data are generated using a model which reproduces the fundamental anatomical features and allows the display method to be assessed.

In the model of the fundus the retina has been represented as a deformed spherical segment containing the separately modelled optic disc on the posterior pole. The retinal blood vessels have been generated using a fractal tree [11] originating from the optic disc. The tree is projected onto the retinal sphere (see Figures 4 and 5). A recursive algorithm generated the vessel trees to a specified level of detail, subject to parameters describing mean branching angle, vessel radii and undulation, and creation of fine lateral vessels which branch from the main vessels at right angles. A repulsion factor was added in order to keep the large vessels from growing near the fovea centralis.

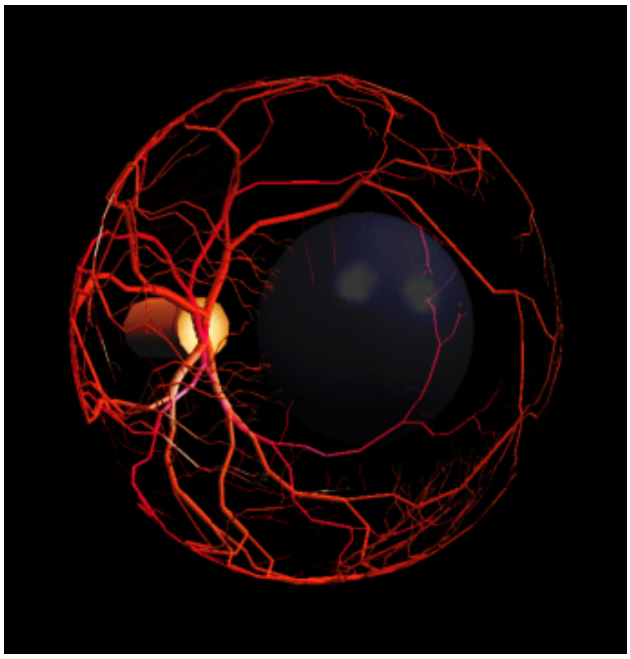

Figure 4: View showing fractal tree of retinal blood vessels (including lens) mapped onto the retinal surface.

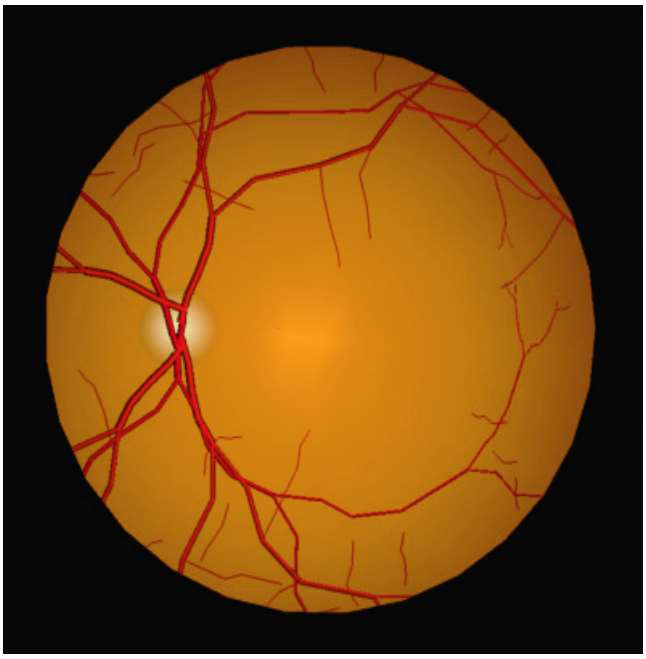

Figure 5: The retina including the optic disc and main blood vessels displayed as would be seen through an ophthalmoscope.

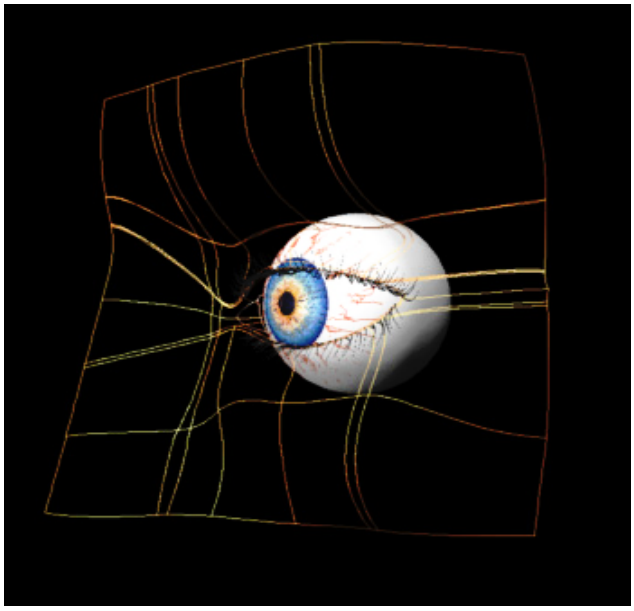

Figure 6: Exterior view of the model with the skin surface rendering omitted.

At the lowest LOD simple line segments are used. At the highest level, the vessels are represented by faceted cylinders replacing the line segments (depending on diameter). At middle levels Gouraud triangular prisms proved to be adequate.

5.4. The eyelids and surrounding face

The eyelids are two thin movable folds, adapted to the front of the eyes and forming an elliptical space when parted. The upper eyelid is larger and more mobile. On the nasal side the eyelids are separated by a triangular space, the lacus lacrimalis (tear lake), which contains a small elevation, the caruncle, and a reddish fold, the plica semilinaris. On the lateral side the eyelids meet at a more acute angle.

Representing the shape of the surface of the skin around the eye presents several problems. There are large smooth areas of tissue, overlapping folds and areas of sharp curvature between the front and rear surfaces of the eyelids. Parametric complexity is desired and surfaces should be flexible and editable: during surgery the eyelids will be stretched open and fixed. Non-uniform rational B-spline (NURBS) surfaces were chosen to model the facial surface for several reasons:

(1) Surfaces are represented with minimal data. Large data sets from patient facial scans may be reduced dramatically by the least squares fitting of a NURBS surface.

(2) NURBS are implemented in hardware on several graphics workstations and evaluation is reasonably fast and stable.

(3) They have a powerful geometric toolkit. The shape is controlled with control points and the continuity with knots. Refinement can be achieved by subdivision and knot addition.

(4) The net formed by the control points approximates the surface. This allows for fast preliminary collision detection between the robot tools and the face.

The initial geometrical data for a patients face is taken from a 3D surface scan. Because the resulting data currently does not give fine enough detail around the eye, and does not give the most efficient representation, a least squares NURBS surface fit of the data is made This represents the basic characteristic features, but with minimal data. An interactive NURBS facial surface editor was written to refine and manipulate the resulting surface. The refinements are made using anatomical data and pictures. Extra knots and control points were added around the eyelid area for fine control over the eyelids and lacus lacrimalis. The multiplicity of the knots along the rim of the eyelids was increased so that the curve between the front and rear faces could be sharpened.

This approach allows the eyelids to be easily manipulated. By moving only a few control points both eyelids can be drawn together and closed (or stretched open and pinned back for operation). Morphing between different settings produces a blinking effect. The portion of the face from the nose to the eyebrow was defined with a 10 x 14 grid of control points. The caruncle and plica semilinaris were created with a small NURBS patch transformed to lie in the lacus lacrimalis. The amount of tessellation of the NURBS is currently dynamically related to viewpoint using the graphics library routines, but we consider it may be faster in some instances to base tessellation on incoming data. A typical configuration of NURBS surfaces representing the skin is shown in Figures 6 and 8.

5.5. The eyelashes

Eyelashes grow as short thick curved hairs from the edges of the eyelids. The upper hairs, more numerous and longer, curve up while those in the lower eyelid curve down so that the upper and lower lashes do not interlace when the eyelids are closed.

The main difficulty in modelling the eyelashes was finding a simple way to describe the length, curl and orientation of each hair. The solution finally arrived at was to represent the 'net' formed by the eyelashes with a piecewise biquadratic mesh having 15 control points (Figure 7), which is attached at one edge via the NURBS eyelid control points in order to move with the eyelids.

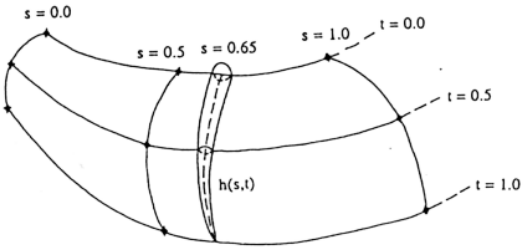

Figure 7: A biquadratic patch used to represent half of the surface used as a basis for constructing the eyelashes.

An editor for the control net was incorporated into the NURBS facial editor. At the highest LOD each hair was then represented by a sequence of truncated cones coaxial with a quadratic curve. A small random factor was added to the quadratic parameters of each hair. The density of hairs is less on the lower eyelid. All these parameters may be adjusted without changing the underlying surface containing the hairs.

6. FINITE ELEMENT MODELLING

At present, analytical development has concentrated on the cornea. To obtain stress distributions in the cornea we use large deformation incompressible 3-D elasticity theory with the equations of equilibrium formulated in spherical polar coordinates. The element geometries are defined in spherical polar coordinates (R,Θ,Φ) in the undeformed state and (r,θ,ϕ) in the deformed state. The polar coordinates Θ,Φ,θ and ϕ have trilinear Lagrange basis functions. The radial coordinates R and r are bicubic Hermite in the normalised material coordinates (ξ_1, ξ_2) lying in the plane of the corneal surface and linear Lagrange in the normalised material coordinate ξ_3 directed transmurally through the corneal thickness (see [7] for details of the finite element technique used here).

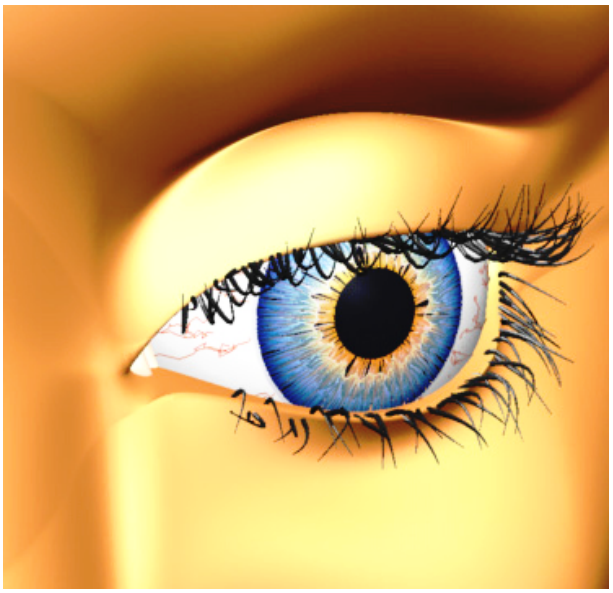

Figure 8: Exterior view of the model showing the NURBS face and the eyelashes.

The material properties are assumed to be homogeneous, orthotropic and nonlinearly elastic with a J-shaped uniaxial stress-strain behaviour along each of the three microstructurally defined axes (assumed to coincide with the r,θ,ϕ directions). Collagen fibres are assumed to lie in the (ξ_1,ξ_2) plane and are given elastic properties typical of the proteoglycan embedded type II collagen fibres found in the bulk of the cornea.

The outside edge of the cornea (limbus) is currently assumed to be fixed in position. In future developments of the model this assumption will be relaxed by including the sclera in the model. Figure 9 shows the finite element model of the cornea with a pressure load applied to the rear surface of the cornea and a point load applied at the centre of the front surface.

7. REPRESENTATION OF ROBOT AND SURGICAL ENVIRONMENT

The surgical environment contains graphical object representations of the robot and ophthalmic surgical tools such as scalpels, clamps for pinning back the eyelids and illumination tools. Each tool can be manipulated from the user interface, by the robot, or by hand using an attached position and orientation tracking device. A sample 'tool path' for the surgeon to cut along has been added, and as the scalpel is moved 3-D arrows appear to direct the surgeon when off path. Other information such as depth of cut and hand tremor are shown in a 'head up display' (see Figure 10). The display of graphic information to aid the surgeon is an open area for future investigation.

8. VIEWING

The observer has complete freedom of viewing position, orientation and field of view. The contents of the scene are chosen from a list of graphical objects. Visibility determination uses criteria based on the viewer's position relative to the model, and on the content of the scene. The LOD for individual objects can be fixed or made dependent on the estimated proportion of the screen that it occupies. In future developments we wish to investigate more sophisticated adaptive display algorithms.

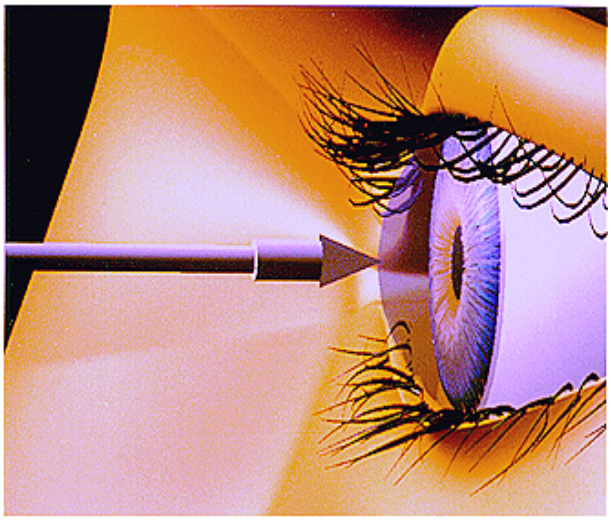

(a)

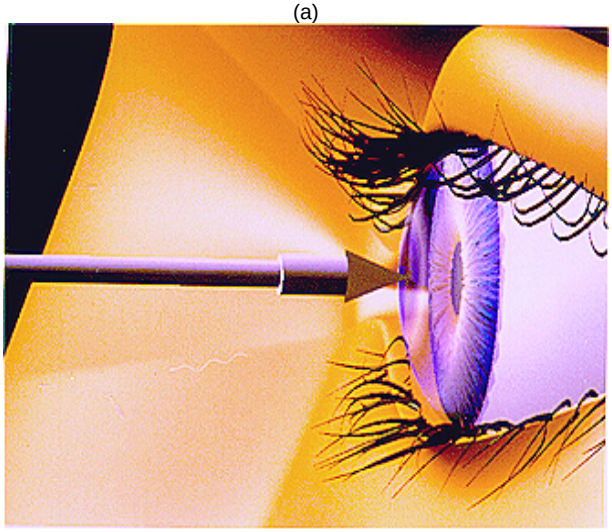

(b)

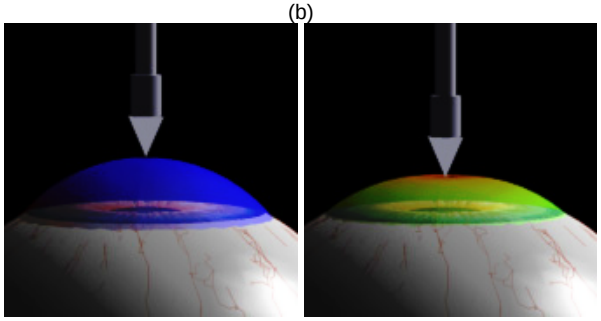

(c) (d)

Figure 9: Views showing the cornea being depressed by a robot probe. In the upper pictures the calculated stress field is displayed with banded colour contours. In the lower pictures the stress field is displayed with an alternative colour map and the facial features have been removed for clarity. (a), (c) Undeformed cornea. (b), (d) Deformed cornea.

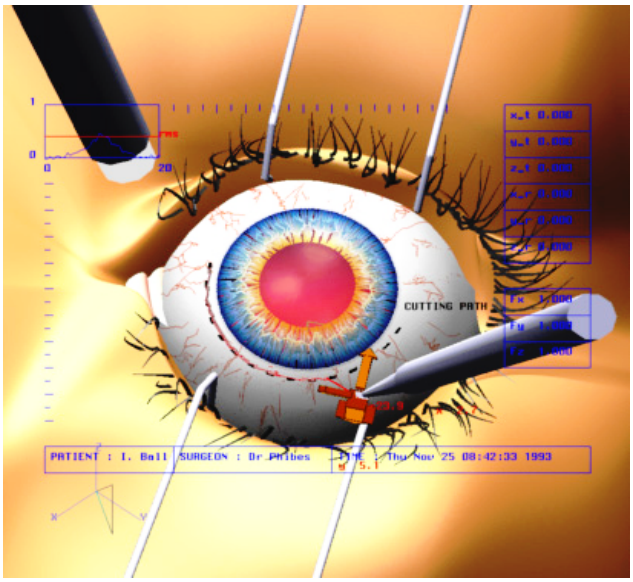

Figure 10: Surgical virtual environment including micro-tools and guidance information. The eyelids have been pulled back as they are during actual surgery. Superimposed on the image is additional information to guide the surgeon. The broken line around the cornea shows a planned cutting path.

At present for stereopsis a time multiplexed stereoscopic display is used with liquid crystal modulator (LCM) shutter glasses. An off-axis projection is made for each eye. Research discussed in [7] has shown that users have differing preferred values for the eye separation parameter usually specified in terms of horizontal viewing angle (HVA), and that this can vary with fatigue. As a result, the user interface includes a control for the HVA. The user interface is included in the stereo display by cloning it for left and right eye views, allowing full control in stereo mode.

9. SOFTWARE DESIGN

The design philosophy was to create a fast and flexible modular system to display both pure graphical data, for visual realism, and graphical data generated from the finite element modelling (at various LOD), so that both visual and mechanical simulation can be combined. Processing is distributed between a finite element module and a graphics module, which may be run in parallel on separate processors (see Figure 10).

The finite element module we have developed (CMISS) is a general purpose program designed to handle large deformation nonlinear elasticity problems. The model is stored as 3-D spherical polar nodal coordinates for both deformed and undeformed geometries, including the Hermite arc-length derivatives, element connectivity data and various basis functions and their derivatives evaluated at Gaussian quadrature points.

The graphics module contains its own reduced representation of the finite element structures including basis functions and connectivity information. After each iteration of the finite element module only changed nodal coordinate data need to be transferred to the graphics module. The complete graphic model is stored as a hierarchical list of graphics objects at various LOD comprised of graphical data which may be independently generated by other software (for example the NURBS editor)

and graphical data generated from the graphics module's finite element structures.

The user has control over the graphics object list and may assign objects different attributes (for example visibility) for different display windows. Several windows containing the same object list can be created allowing different viewing setups simultaneously The graphic object list is traversed and the selected objects are displayed according to visibility and LOD criteria as described previously. Dynamic data structures are used to store objects and data are referenced through pointer structures for minimum reassignment.

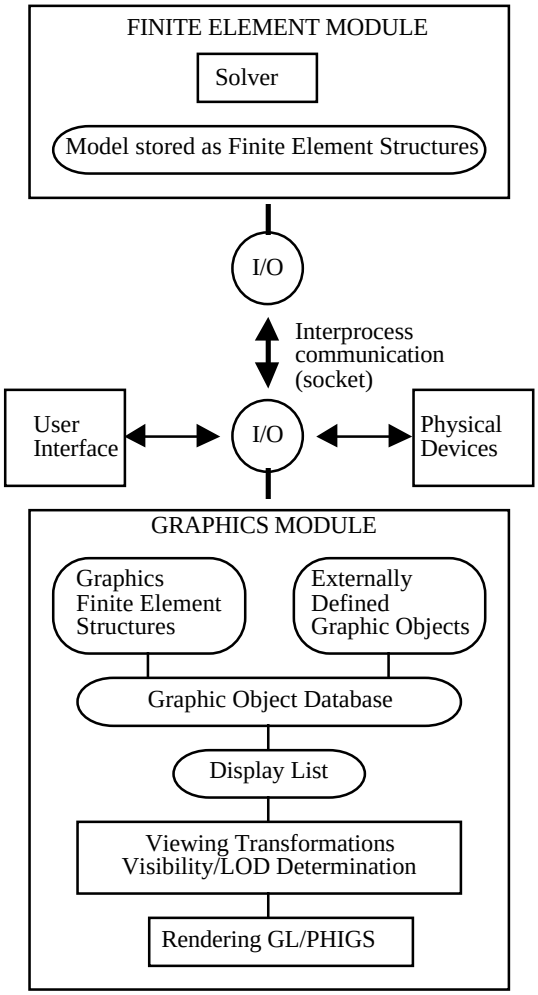

Figure 11: Organisation of the software.

10. SOFTWARE IMPLEMENTATION

The graphics module has been written in the C language for environments running the X window system with the Motif widget set for the user interface and Silicon Graphics' GL graphics library. The finite element software (CMISS) has been developed in Fortran.

Hardware resources used during software development included an IBM RISC/6000 Model 730 graphics system and a Silicon Graphics R4000 IRIS Indigo desktop workstation. The latter workstation has a 120 Hz switched display with Crystal EYES liquid crystal shutter glasses for stereoscopy. A DEC Alpha 3000/300 was also used for the finite element analysis processing. A Silicon Graphics Reality Engine has since been used for a graphics speed trial.

11. RESULTS AND DISCUSSION

The virtual environment generates stereoscopic 3-D representations of the robot micro-tools, the main macroscopic features of the eyeball and the surrounding face. The eyeball can move, the eyelids can blink or be stretched open, and the pupil can be made to contract or dilate. The eye model is coupled to a finite element model of the corneal tissue, which can be used to generate realistic deformations and stress fields. Each graphical object has been generated parametrically, allowing arbitrary complexity to be used for differing LOD.

Positional information for the virtual micro-tools from the microsurgical robot and 3-D devices coupled to various hand held surgical tools is used to manipulate the virtual representations.

Initial results indicate a satisfactory level of realism with graphic display speeds on a desktop workstation in the order of what is required. Adequate display speeds are achieved on a high end workstation for the prototype micro-surgical robotic system. At present an incremental update of the computed displacement and stress field takes about one second on an Alpha 3000/300 workstation. This level of performance is acceptable as we anticipate the surgeon making an incision and pausing to evaluate the consequences before proceeding. To assess performance on a high end workstation, the system has been run on a Silicon Graphics Reality Engine. It achieved graphic update rates significantly greater than 10Hz interactively displaying the model together with a 3-D position and orientation tracked surgical tool.

11.1 Examples

All examples and display performance times given below were produced on a *desktop* workstation used during the development, a Silicon graphics R4000 IRIS Indigo with a GR2-XS24 graphics board with Z-buffer.

Example	Polygons (quads)	Line segs.	NURBS tessellation	Update time (s)
Figure 12(a) eyeball exterior	2490	900	-	0.11
+ eyelashes, NURBS	5690	900	50 pixels	0.42
Figure 12(b) eyeball exterior	1155	225	-	0.04
+ eyelashes, NURBS	2115	225	100 pixels	0.21
Figure 5 eyeball interior	2280	2016	-	0.18

Table 1: Total display update times on a desktop workstation.

11.2 Complexity adjustment

The complexity of all aspects of the model can be easily adjusted. Figure 12 shows two close up views of the front of the eye. The level of detail versus display update time appears to be approximately linear. As shown (see Table 1), for only a slight reduction in apparent quality, the complete image in Figure 12(b) can be rendered in approximately half the time required for Figure 12(a).

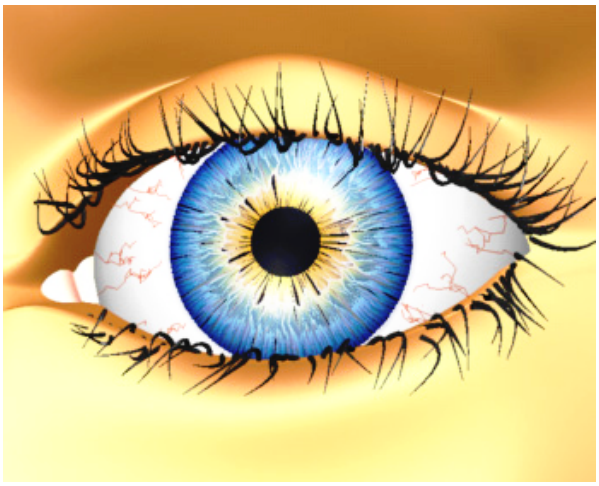

(a)

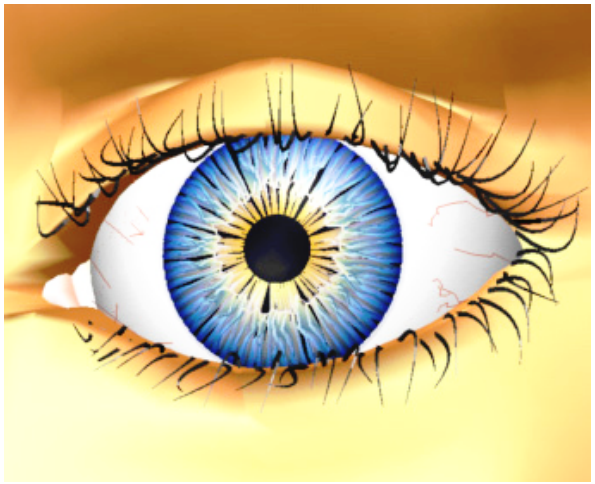

(b)

Figure 12: Close up views of the eye with different complexity parameter values.
(a) Same complexity as used for Figures 8, 9 and 10.
(b) All parameters reduced by a factor of two relative to (a).

12. CONCLUSIONS

A surgical virtual environment containing a detailed model of the eye has been implemented for use in a teleoperated micro-surgical robotic system for eye surgery. Visual and mechanical simulations have been combined by the coupling of parametrically defined graphic realism and finite element analysis. The virtual environment produces a fair level of realism (adjustable) for a low display regeneration time on a desktop workstation and gives sufficiently fast performance (>10Hz) on a high end workstation. It now forms part of a prototype micro-surgical robotic system.

Interest has been expressed in using the model for anatomic teaching, as it allows students to select and view each anatomical structure individually.

The model contains a large elastic deformation finite element representation of the cornea which computes the deformation and stress fields for a given displacement or load applied to the cornea. Extensions will include an analysis of the optical properties of the deformed cornea. We will also include tissues surrounding the eye in the graphic model. Eventually we intend to model a number of complete surgical procedures.

ACKNOWLEDGEMENTS

Financial support from the University of Auckland Research Committee, and the New Zealand Lottery Grants Board is gratefully acknowledged.

REFERENCES

[1] Baillie, J., Jowell, P., Evangelou, W. and Bickel, W. Use of computer graphics simulation for teaching of flexible sigmoidoscopy. *Endoscopy 23*, (1991), 126-129.

[2] Chen, D.T. and Zeltzer, D. Pump it Up: Computer animation of a biomechanically based model of muscle using the finite element method. Proceedings of SIGGRAPH '92 (Chicago, Illinois, July 26-31, 1992), In *Computer Graphics*, 26, 2, (July 1992), 89-98.

[3] Delp, S. Loan, P., Hoy, M., Zajac, F., Fisher, S. and Rosen, J. An Interactive graphics-based model of the lower extremity to study orthopaedic surgical procedures. *IEEE Transactions on Biomedical Engineering, 37*, 8, (1990).

[4] Hasimoto, D., Dohi, T., Tzuzuki, M., Horiuchi, Y., Chinzei, K., Suzuki, M. and Idezuki, Y. Development of a computer aided surgery system: Three dimensional graphic reconstruction for treatment of liver cancer. *Surgery*, (1991), 589-596.

[5] Hodges, L.F. Time multiplexed stereoscopic computer graphics. *IEEE Computer Graphics and Applications*, (March 1992), 20-30.

[6] Huang, T., Bisarnsin, T., Schachar, R.A., Black, T.D. Corneal curvature change due to structural alternation by radial keratotomy. *Journal of Biomechanical Engineering*, 110, (1988), 249-253.

[7] Hunter, P.J. and Smaill, B.H. The analysis of cardiac function: a continuum approach. *Prog. Biophys. Molec. Biol. 52*, (1989) 101-164.

[8] Hunter, I.W., Jones, L.A., Sagar, M.A., Doukoglou, T.D., Lafontaine, S.R., Charette, P.G., Mallinson G.D., Hunter, P.J. A teleoperated microsurgical robot and associated virtual environment for eye surgery, *Presence*, (Accepted 1994)

[9] Magnenat-Thalmann, N. and Thalmann, D. *Synthetic Actors in Computer Generated 3D films*. Springer-Verlag, (1990).

[10] Maurice, D.M. Mechanics of the cornea. *The Cornea: Transactions of the World Congress on the Cornea III*. Ed. H. Dwight Cavanagh. Raven Press Ltd., (1988).

[11] Oppenheimer, P.E. Realtime design and animation of fractal plants and trees. Proceedings of SIGGRAPH '86 (New York). In *Computer Graphics* 20, 4, (1986), 55-64.

[12] Pieper, S., Rosen, J. and Zeltzer, D. Interactive graphics for plastic surgery, Proceedings of SIGGRAPH '92 (Chicago, Illinois, July 26-31, 1992), In *Computer Graphics*, 26, 2, (July 1992), 127-134.

[13] Pinksy, P.M.,Datye, D.V. A Microstructurally based finite element model of the incised human cornea. *J. Biomechanics 24*, 10, (1991), 907-922.

[14] Sims, D. The Point where Lines Converge.. *IEEE Computer Graphics and Applications, 13*, July (1993), 7-9.

[15] Young, A.A. and Hunter, P.J. Epicardial surface estimation from coronary angiograms. *Computer Vision, Graphics, and Image Processing 47*, (1989) 111-127.